Increased Brownian Force Noise from Molecular Impacts in a Constrained Volume

A. Cavalleri,[1] G. Ciani,[2] R. Dolesi,[2] A. Heptonstall,[3] M. Hueller,[2] D. Nicolodi,[2,*] S. Rowan,[3] D. Tombolato,[2] S. Vitale,[2] P. J. Wass,[2] and W. J. Weber[2]

[1]*Centro Fisica degli Stati Aggregati, 38123 Povo, Trento, Italy*

[2]*Dipartimento di Fisica, Università di Trento, and INFN Gruppo di Trento, Via Sommarive 14, 38123 Povo, Trento, Italy*

[3]*University of Glasgow, Glasgow G12 8QQ, United Kingdom*

(Received 31 July 2009; published 28 September 2009)

We report on residual-gas damping of the motion of a macroscopic test mass enclosed in a nearby housing in the molecular flow regime. The damping coefficient, and thus the associated thermal force noise, is found to increase significantly when the distance between the test mass and surrounding walls is smaller than the test mass itself. The effect has been investigated with two torsion pendulums of different geometry and has been modeled in a numerical simulation whose predictions are in good agreement with the measurements. Relevant to a wide variety of small-force experiments, the residual-gas force noise power for the test masses in the LISA gravitational wave observatory is roughly a factor 15 larger than in an infinite gas volume, though still compatible with the target acceleration noise of 3 fm s^{-2} $Hz^{-1/2}$ at the foreseen pressure below 10^{-6} Pa.

DOI: 10.1103/PhysRevLett.103.140601 PACS numbers: 05.40.Jc, 07.10.Pz, 95.55.Ym

The fluctuation-dissipation theorem [1] states that any system with dissipation exhibits fluctuations analogous to Brownian motion that can be modeled with an external driving force with a power spectral density

$$S_F(\omega) = 4kT\mathrm{Re}\left(\frac{\partial F}{\partial v}\right) = 4kT\mathrm{Re}[Z(\omega)] \qquad (1)$$

where k is Boltzmann's constant, T is the temperature of the system, and $Z(\omega)$ is the mechanical impedance of the system. These equilibrium fluctuations are a fundamental limit of precision metrology experiments employing macroscopic test masses nominally in perfect free fall to define geodesic reference frames.

An unavoidable source of dissipation comes from residual gas in the experimental volume, which yields a viscous, frequency independent, impedance $Z(\omega) = \beta$. Theoretical calculations for small-force experiments [2–4] and direct observations [5,6] show the gas-damping coefficient β to be proportional to residual-gas pressure P and to some effective surface area, which depends on the test mass geometry.

A recent calculation [7] for a cubic test mass has found that the translational damping coefficient is

$$\beta_{\mathrm{tr}}^{\infty} = Ps^2\left(1 + \frac{\pi}{8}\right)\left(\frac{32m}{\pi kT}\right)^{1/2} \qquad (2)$$

where s is the side length of the test mass, and m is the mass of the gas molecules. For rotation, relevant for the experiments we will present shortly, the coefficient is

$$\beta_{\mathrm{rot}}^{\infty} = Ps^4\left(1 + \frac{\pi}{12}\right)\left(\frac{2m}{\pi kT}\right)^{1/2}. \qquad (3)$$

This calculation assumes that gas and test mass are in thermodynamic equilibrium, that gas molecule collisions with the test mass are completely inelastic, with prompt stochastic reemission from the surface with a Maxwell-Boltzmann velocity distribution and cosine law angular distribution. Importantly, this and other calculations assume that the test mass is surrounded by an infinite volume of collisionless gas, hence the superscript ∞, such that a molecule emitted from the test mass surface disappears into the surrounding volume, and that the momentum it imparts on the test mass is uncorrelated with any subsequent collisions. This assumption breaks down when the distance between the test mass and the surrounding enclosure is only a fraction of the test mass size, as in the geometry studied here, where the gap is roughly one tenth of the test mass size.

Our experimental setup probes small forces relevant to the quality of free fall achievable for the test masses of the Laser Interferometer Space Antenna (LISA) gravitational-wave observatory [8,9] and its precursor LISA Pathfinder [10], using a torsion pendulum. External force disturbances are suppressed to a level where the thermal noise plays an important role in limiting the force sensitivity. Measurements of the torsion pendulum free-motion damping show a residual-gas contribution several times larger than predicted by the infinite-volume model, accompanied by an observed noise increase consistent with mechanical thermal noise. We present here simple arguments, based on the impedance to stochastic molecular flow through the small gaps around the test mass, supported by numerical simulation, that quantitatively explain this observed increased dissipation. Enhanced gas damping has also been observed in micro-mechanical resonators [11], though the interpretations have employed an elastic model of the molecule-wall interaction [12].

Two different torsion pendulum geometries are used for the experimental investigation. Both suspend a hollow replica of the LISA Pathfinder cubic test mass with side

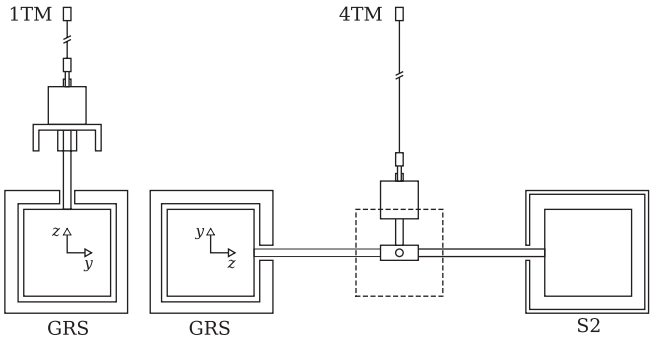

FIG. 1. Sketch of the 1TM and 4TM pendulum inertial members surrounded by the GRS. Test mass side is 46 mm. Gaps between test mass and GRS are 4.0, 2.9, and 3.5 mm on, respectively, the x, y, and z faces. The $S2$ gaps are 8.0, 6.0, and 8.0 mm gaps on x, y, and z faces, respectively.

length $s = 46$ mm inside a prototype of the LISA Pathfinder Gravity Reference Sensor (GRS) [13] that completely surrounds the test mass. All GRS, test mass, and other inertial member surfaces are gold coated. In the 1TM torsion pendulum , the rotation axis coincides with the test mass z axis of symmetry, as shown on the left of Fig. 1. In the 4TM torsion pendulum [16,17], the test mass enclosed by the GRS is one of four identical test masses in a cross shaped configuration, suspended off-center with respect to the fiber axis with a $r = 0.1065$ m arm, as shown on the right of Fig. 1. The opposite test mass is enclosed in a similar capacitive sensor ($S2$), featuring larger gaps. The 4TM pendulum employs a 50 μm diameter tungsten fiber, while the 1TM pendulum uses a 40 μm fused silica fiber with much lower internal dissipation. Both torsion pendulums facilities operate at the temperature of 293 K, controlled within 0.1 K.

For both pendulums, we have measured the torsional damping coefficient in the pressure range of roughly 0.003–3 m Pa (mean free paths of order 10 km down to 10 m), by direct measurement of the amplitude decay time τ of the free pendulum motion

$$\beta = -\frac{\partial N}{\partial \dot{\varphi}} = \frac{2I}{\tau} \tag{4}$$

where I is the torsion pendulum moment of inertia. The decay time is computed as the average of the ratio between oscillation amplitude, with each amplitude point averaged over three periods, and its time derivative, as estimated by the difference between successive points. Uncertainty is computed on a statistical basis.

Measurements were typically performed over 1–3 days, using large initial amplitudes of order mrad. No amplitude dependence of τ was observed. The 1TM and 4TM oscillation periods were roughly 460 and 1400 s, respectively, and their ring-down times in the limit of zero pressure were roughly 6 years ($Q \simeq 1.2 \times 10^6$) and 16 days ($Q \simeq 3.2 \times 10^3$). In the case of the 4TM torsion pendulum, we performed the measurement both with and without the GRS around the test mass.

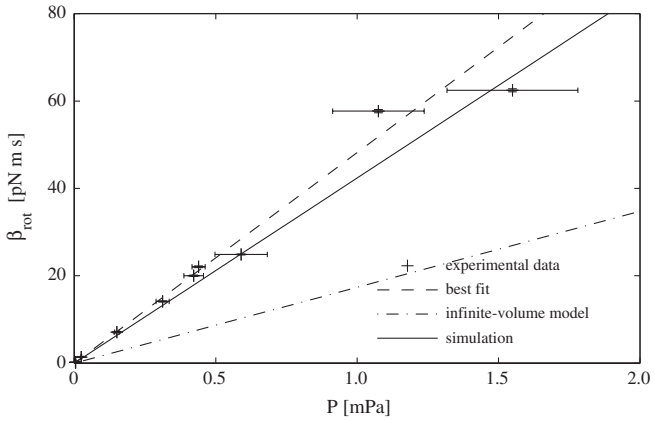

FIG. 2. Measured 1TM gas-damping coefficients β_{rot} as function of residual-gas pressure P. Infinite-volume model and simulation predictions are also shown.

The pressure in the torsion pendulum vacuum chambers is measured with ion gauges cross calibrated with a certified pressure gauge whose accuracy is within 15%, employing the calibration factor recommended for air. While we have not as yet identified the dominant gas species in our chamber, measurements with the same apparatus have confirmed the pressure-dependent radiometric effect model [15,18] at the 10% level, indicating similar systematic uncertainty in the pressure measurements here.

The measured damping coefficients, plotted in Figs. 2 and 3, are found to depend linearly on pressure. The residual zero-pressure intercept, from other dissipation mechanisms, has been removed from both datasets, and the pressure dependence is summarized in Table I. The 1TM data can be directly compared with the infinite-volume prediction in Eqn. (3). The 4TM prediction is calculated from the rotational and translational contributions, $\beta = 4(r^2\beta_{tr}^{\infty} + \beta_{rot}^{\infty})$. The infinite-volume model predictions are several times smaller than the measured values and would foresee no difference caused by the

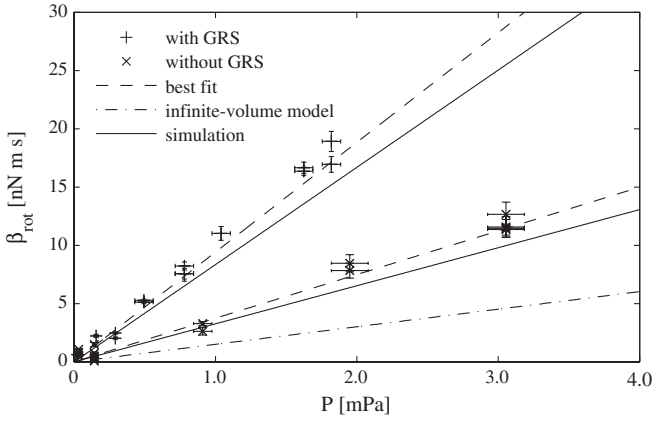

FIG. 3. Measured 4TM gas-damping coefficients β_{rot} as function of residual-gas pressure P, with and without the GRS surrounding one of the test masses. Infinite-volume model and simulation predictions are also shown.

TABLE I. Comparison of β pressure dependence, obtained from measurement, infinite-volume model, and simulation, in different configurations: I. 1TM, II. 4TM with GRS, III. 4TM without GRS, IV. 4TM GRS contribution, obtained as difference between configurations II and III. Simulation uncertainties are on the fourth significative digit.

	measurement	∞ model	simulation
	$\partial\beta/\partial P$ [m^3 s]	$\partial\beta/\partial P$ [m^3 s]	$\partial\beta/\partial P$ [m^3 s]
I.	$(4.8 \pm 0.1) \times 10^{-8}$	1.74×10^{-8}	4.24×10^{-8}
II.	$(9.4 \pm 0.2) \times 10^{-6}$	1.51×10^{-6}	7.87×10^{-6}
III.	$(3.7 \pm 0.1) \times 10^{-6}$	1.51×10^{-6}	3.27×10^{-6}
IV.	$(5.7 \pm 0.3) \times 10^{-6}$	0	4.60×10^{-6}

removal of the GRS, while here it lowers the total 4TM damping by more than a factor two.

A series of torque noise measurements, performed with the 1TM pendulum, has confirmed the Brownian nature of the gas-damping noise. Measurements were performed at six different pressures, from $P_0 = 0.004$ to 15 mPa. Torque noise was estimated with a dual-readout cross-correlation technique [14,15]. For each measurement, lasting 1–3 days, noise spectra were averaged over 8 to 20 windows of 25 000 s each, with 50% overlap and over logarithmically spaced frequency bins, with uncertainties estimated as the standard deviation divided by the square root of the number of points. To identify the gas-damping noise, the P_0 spectrum was subtracted from the five higher pressure measurements, yielding a differential spectrum ΔS_N for each $\Delta\beta \equiv \beta(P) - \beta(P_0)$. Two such spectra are shown in the inset of Fig. 4. The gas-damping noise is best fit by a white noise model between 0.5 and 12 mHz, where the gas-damping noise is resolved. The averages of each differential spectrum in this bandwidth are plotted as a function of $\Delta\beta$ in Fig. 4, with a linear fit yielding $\Delta S_N = (1.08 \pm 0.03) \times 4kT\Delta\beta$. The gas-damping noise is thus white and within 10% of the Brownian noise prediction.

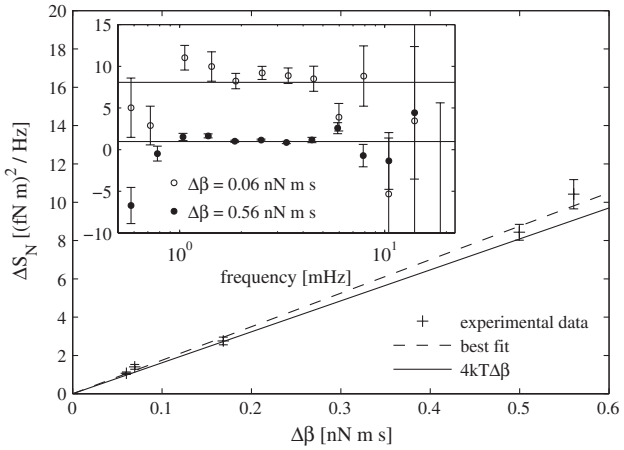

FIG. 4. Measured averaged gas-damping noise difference ΔS_N in the band 0.5–12 mHz as a function of differential damping coefficient $\Delta\beta$, compared with the Brownian noise prediction. Inset shows two noise spectra, compared against the predicted noise level.

The excess gas-damping and associated force noise, well above that foreseen by the infinite-volume model, is caused by the nearby GRS walls, as can be understood by a simple picture of molecular gas flow. Test mass motion along the x direction, with velocity v, requires gas flow Q, expressed in Pa m^3 s^{-1}, from the volume on one x face to the other, to restore pressure equilibrium. The finite molecular flow conductance C of the channels, provided by the electrode-housing y and z faces gaps, requires a pressure drop ΔP to maintain this gas flow. In steady state conditions, $Q = Ps^2v$, and thus the pressure drop must be $\Delta P = Q/C = Ps^2v/C$. The test mass is thus subject to a force, $F = \Delta P s^2$, proportional to the velocity v, and thus to an increase in the viscous damping

$$\beta = \left|\frac{\partial F}{\partial v}\right| \approx \frac{Ps^4}{C}. \tag{5}$$

Gas flow in a finite conductance is a dissipative process.

In an equivalent picture from the standpoint of the associated force noise, the flow impedance of the channels is related to the time needed for molecules to random walk from one side of the test mass to the other. This random walk requires repeated impacts of a single molecule on the same test mass face and thus introduces correlations between subsequent collisions, with repeated force impulses of the same sign slowing the averaging out of the net force and thus increasing force noise.

To verify our hypotheses, we developed, on the same assumptions as the infinite-volume model, a numerical simulation of the gas dynamics within a simplified geometry of a cubic test mass inside a cubic housing. The gas is supposed to be composed of a single specimen with molecular mass of 30 amu. The simulation is composed of N steps, simulating each one the dynamics of a single molecule. The simulation allows the system to evolve for a time Δt chosen long enough to allow time for the molecules to stochastically move many times from one side of the test mass to the other. Momentum exchange between test mass and gas molecules is recorded at each collision. The gas-damping coefficient β is computed from the variance σ_F^2 of each component of the total force acting on the test mass:

$$\beta_{\mathrm{tr}}^{\mathrm{sim}} = \frac{S_F}{4kT} = \frac{\Delta t}{2kT}\sigma_F^2. \tag{6}$$

An equivalent approach is used to calculate $\beta_{\mathrm{rot}}^{\mathrm{sim}}$ from the mean square fluctuation of the torque.

The simulation has been performed as a function of gap size, with the results shown in Fig. 5. In addition to confirming the analytic model in Eqns. (2) and (3) for large gaps, the data show the expected increased damping for $d \lesssim s$, which approaches a power law $(d/s)^{-2}$ for vanishing gap. This can be roughly understood with the flow impedance arguments presented earlier. For $s \gg d$, the channel conductance is of order $C \approx d^2 \ln(s/d) \times (kT/m)^{1/2}$ [19]. Substituting into Eqn. (5) and comparing with Eqn. (2),

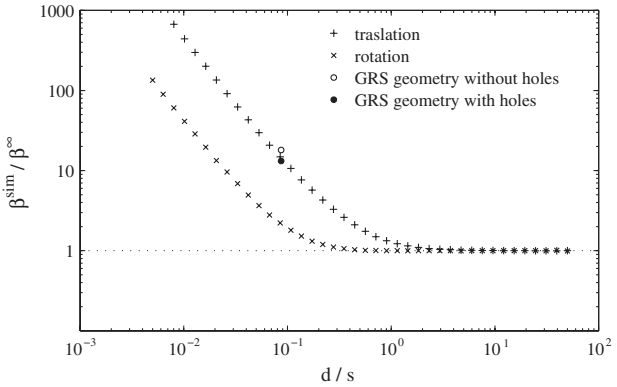

FIG. 5. Gas damping β^{sim} obtained from the numerical simulation for different test mass side lengths s and gap sizes d, normalized to the infinite-volume model prediction β^{∞}.

$$\beta_{\mathrm{tr}} \approx \frac{\beta_{\mathrm{tr}}^{\infty}}{\ln(s/d)(d/s)^2}. \quad (7)$$

This asymptotically approaches a log slope of -2 for vanishing gap, as observed in the simulation data.

Figure 5 also shows simulation results obtained simulating the slightly asymmetric gaps of the real GRS geometry. Finally, we also simulate the 6 mm diameter holes present on the x faces, which act as vents that reduce the damping pressure head, with a roughly 20% reduction of the gas damping obtained in the simulation.

The measured 1TM gas-damping coefficient can be directly compared with the simulation results, adding in small contributions due to minor features of the inertial member computed with the infinite-volume model. The gas-damping coefficient for the 4TM torsion pendulum without the GRS is computed from simulation results for the $S2$ geometry and from the infinite-volume model for the other three test masses $\beta = 3(r^2\beta_{\mathrm{tr}}^{\infty} + \beta_{\mathrm{rot}}^{\infty}) + r^2\beta_{\mathrm{tr}}^{\mathrm{sim}} + \beta_{\mathrm{rot}}^{\mathrm{sim}}$. The GRS contribution in the 4TM gas-damping coefficient is computed from simulation results and infinite-volume model predictions $\beta = r^2(\beta_{\mathrm{tr}}^{\mathrm{sim}} - \beta_{\mathrm{tr}}^{\infty}) + (\beta_{\mathrm{rot}}^{\mathrm{sim}} - \beta_{\mathrm{rot}}^{\infty})$. Results are summarized in Table I. The agreement with measurements is within 20%. This is good in respect to the approximations in the geometrical model of the GRS contained in the simulation. We note that in the 4TM pendulum, the gas-damping coefficient is dominated by the translational part, the rotational one accounting only for roughly 1% of the total, and thus the 4TM measurement validates the translational damping relevant to force noise.

Converting the simulated residual-gas Brownian force-noise into acceleration noise for LISA and LISA Pathfinder, with a 2 kg test mass, yields

$$S_a^{1/2} = 1.3 \times 10^{-15}\left(\frac{P}{10^{-6}\ \mathrm{Pa}}\right)^{1/2} \mathrm{m\,s^{-2}\,Hz^{-1/2}}. \quad (8)$$

Equation (8) is compatible with the target acceleration noise of LISA Pathfinder and LISA, the latter of which will operate at pressure below 10^{-6} Pa, reached by venting the GRS to space [8]. Gas damping is likely to be the dominant pressure-related force noise for LISA. We note that, unlike many force-noise sources, Brownian noise from residual gas does not improve at higher frequencies; this is important for future gravitational-wave missions, such as DECIGO and BBO, whose ambitious sensitivity goals near 0.1 Hz and shorter interferometry arms require even lower acceleration noise limits [20,21]. Finally, the gas-damping question effectively confirms the need, also based on electrostatic concerns [13], for gaps of at least several mm: for a similar sized test mass and gaps of 0.3 mm, roughly the gap employed in several space accelerometry missions [22,23], the resulting acceleration noise from this source alone would be an order of magnitude above the LISA goal.

*nicolodi@science.unitn.it

[1] H. B. Callen and R. F. Greene, Phys. Rev. **86**, 702 (1952).
[2] L. D. Hinkle and B. R. F. Kendall, J. Vac. Sci. Technol. A **10**, 243 (1992).
[3] B. L. Schumaker, Classical Quantum Gravity **20**, S239 (2003).
[4] P. R. Saulson, Phys. Rev. D **42**, 2437 (1990).
[5] C. A. Hagedorn, S. Schlamminger, and J. H. Gundlach, in *Proc. of the Laser Interferometer Space Antenna: 6th International LISA Symposium, Greenbelt, Maryland*, AIP Conf. Proc. No. 873 (AIP, New York, 2006)189.
[6] K. Numata, J. Horowitz, and J. Camp, Phys. Lett. A **370**, 91 (2007).
[7] A. Cavalleri *et al.*, arXiv:0907.5375v1.
[8] P. Bender *et al.*, LISA: A Cornerstone Mission for the Observation of Gravitational Waves (ESA-SCI, 2000, 11, System and Technology Study Report).
[9] S. Vitale *et al.*, Nucl. Phys. B, Proc. Suppl. **110**, 209 (2002).
[10] S. Anza *et al.*, Classical Quantum Gravity **22**, S125 (2005).
[11] J. D. Zook *et al.*, Sens. Actuators. A Phys. **35**, 51 (1992).
[12] Minhang Bao, Heng Yang, Hao Yin, and Yuancheng Sun, J. Micromech. Microeng. **12**, 341 (2002).
[13] R. Dolesi *et al.*, Classical Quantum Gravity **20**, S99 (2003).
[14] L. Carbone *et al.*, Phys. Rev. D **75**, 042001 (2007).
[15] A. Cavalleri *et al.*, Classical Quantum Gravity **26**, 094017 (2009).
[16] A. Cavalleri *et al.*, Classical Quantum Gravity **26**, 094012 (2009).
[17] L. Carbone *et al.*, in *Proc. of the Laser Interferometer Space Antenna: 6th International LISA Symposium*, AIP Conf. Proc. No. 873 (AIP, New York, 2006), 561.
[18] L. Carbone *et al.*, Phys. Rev. D **76**, 102003 (2007).
[19] R. G. Livesey, Vacuum **76**, 101 (2004).
[20] S. Kawamura *et al.*, Classical Quantum Gravity **23**, S125 (2006).
[21] J. Crowder and N. J. Cornish, Phys. Rev. D **72**, 083005 (2005).
[22] D. Hudson, R. Chhun, and P. Touboul, Adv. Space Res. **39**, 307 (2007).
[23] M. D. Drinkwater *et al.*, in *Proc. 3rd Int. GOCE User Workshop, 6-8 November 2006, Frascati, Italy* (ESA Special Publication SP-627, 2007).